Supporting Information

Han et al. 10.1073/pnas.1500458112

SI Materials and Methods

Plasmid Engineering. For the cRNA expression constructs, iGluR coding sequences were PCR-amplified from full-length cDNAs as follows: GluRIIA residues L24-S907 from RE27895, GluRIIB residues N19-K913 from the published cDNA clone (1), GluRIIC residues Q48-V965 from GH22844, GluRIID residues F20-D902 from RE24732, and GluRIIE residues Q23-Q897 from RE07945. The iGluR sequences were placed by QuikChange mutagenesis between the Tolloid-related signal peptide MRRRRGTPLGVS-WTNCVLLLATGLLVVLISVHA (2) and an $RGSH_6$ C-terminal tag, cloned into the pSP64 expression vector. For chemiluminescence assays, an HA-tag was added (by PCR and QuikChange mutagenesis) to each of the iGluR subunits in between the signal peptide and the N-terminal domain. For the Neto β cRNA expression, the full-length coding sequence from RE42119 was cloned into pSP64.

The pSP64-based constructs were linearized with XbaI, and the cRNA synthesized using SP6 polymerase (Ambion, mMessage mMachine transcription kit). Defolliculated stage 5–6 *Xenopus* oocytes obtained from Ecocyte Bioscience were injected with between 0.5 ng to 10 ng of cRNA as indicated, and incubated at 18 °C for 2–4 d in ND96 (96 mM NaCl, 2 mM KCl, 1.8 mM $CaCl_2$, 1 mM $MgCl_2$, 5 mM Hepes, 2.5 mM sodium pyruvate, gentamycin at 50 μg/mL, pH 7.6).

Immunohistochemistry and Surface Labeling. Three days after injection with 2 ng of each cRNA, oocytes were fixed overnight at 4 °C in PBS containing 4% (vol/vol) formaldehyde (Polysciences) and 15% (vol/vol) picric acid (Electron Microscopy Sciences); uninjected control oocytes from the same batch were processed identically. Fixed oocytes were washed in PBS with 0.5% Triton X-100 over 8 h, then incubated overnight with primary antibodies at 4 °C in PBS with 0.5% Triton X-100. Primary antibodies were used at the following dilutions: mouse anti-$RGSH_6$ (Qiagen), 1:100; rat anti-HA (3F10, Roche), 1:100, rat anti–Neto-ex, 1:200 (3). Alexa Fluor 488- and Alexa Fluor 568-conjugated secondary antibodies (Molecular Probes; 1:200) were incubated for 1 h at room temperature or overnight at 4 °C. The oocytes were next cryoprotected by overnight immersion in PBS with 30% (wt/vol) sucrose and embedded in media for frozen sectioning (Fischer Scientific). Next, 20-μm sections were cut on a freezing microtome and were mounted in ProLong Gold (Invitrogen). Sections from oocytes injected with different cRNAs or uninjected controls were imaged under identical confocal settings in the same imaging session with a laser scanning confocal microscope (CarlZeiss LSM780).

The level of cell surface HA-tagged iGluRs was measured by chemiluminescence as previously described (4). Briefly, 3 d after injection, oocytes were blocked for 30 min with 1% BSA in ND96 solution, then incubated for 1 h with 0.25 μg/mL rat anti-HA antibody (3F10, Roche), washed with ND96 containing 1% BSA, followed by 1 h incubation with horseradish peroxidase-conjugated secondary antibody (1:400; Jacksons Laboratories). All incubations and washes were performed at 4 °C. Individual oocytes were placed into a mixture of 70 μL ND96 and 30 μL of SuperSignal ELISA Femto maximum sensitivity substrate (Pierce) and incubated for 1 min. The chemiluminescence signal was integrated for 2 s and quantified using a Monolight 3010 Luminometer (BD Biosciences).

Electrophysiology. Two-electrode voltage-clamp recordings at a holding potential of −60 mV, with 3M KCl agarose-tipped electrodes of resistance 0.1–0.8 MΩ were performed as described previously (5), 2–3 d after injection of cRNAs, typically 1 ng of each subunit with 1 ng Neto β. The bath solution contained 100 mM NaCl, 1 mM KCl, 5 mM Hepes pH 7.5, to which $BaCl_2$, $CaCl_2$ and $MgCl_2$ were added as required. Con A (Sigma Type IV), 0.6 mg/mL dissolved in recording solution and 0.2-μm filtered was applied for 4 min after oocytes were impaled to block desensitization. Amino acid ligands and NASPM purchased from Tocris Bioscience were dissolved in recording solution and applied by computer operated solenoid valves. ATX was a gift from Koji Nakanishi, Columbia University, New York, NY.

Protein Expression. The GluRIIB LBD S1S2 construct, residues D416-K537 and D660-D802, connected by a GT dipeptide linker with an N-terminal MH_8LVPRGS affinity purification tag and thrombin cleavage site, was created by overlap PCR from the full-length cDNA and cloned into the pET22 expression vector used previously for expression of other iGluR S1S2 constructs (6). Protein was expressed in origami B(DE3) cells induced overnight with 30 μM isopropyl-β-D-thiogalactopyranoside at 18 °C; final yields following immobilized metal-ion affinity chromatography and anion-exchange chromatography, with thrombin cleavage used to remove the affinity tag, were typically 1.6 mg/L. Similar constructs were also prepared for GluRIIA, GluRIIC, GluRIID, and GluRIIE, but only GluRIIA gave soluble protein, and attempts to obtain diffraction quality crystals have not been successful.

Crystallography. Crystals were grown at 20 °C by repeated rounds of microseeding from a protein stock of concentration 5.5 mg/mL in a buffer of composition 150 mM NaCl, 10 mM Tris pH 8.0, 1 mM EDTA, and 2 mM L-glutamate, with a reservoir containing 18% PEG MME 2K, 0.1 M Tris, pH 8.0, 5 mM $NiCl_2$. X-ray diffraction data were collected at beam line ID22 at the Advanced Photon Source using a MAR 300 mosaic CCD detector (Table S1) and processed using HKL2000 (7). Using the GluK2 LBD glutamate complex PDB ID code 1S50 as a probe, a solution with two molecules in the asymmetric unit, with a strong NCS peak, was obtained by molecular replacement using PHASER (8), RFZ = 6.5, TFZ = 11.9 + TNCS, LLG = 354, NCS translation vector = 0.490 0.455 0.497. An R_{free} set was picked using thin shells and the structure refined using PHENIX (9) with manual rebuilding using COOT (10). The final model was refined to an R_{free} value of 22.9% with good geometry at a resolution of 2.0 Å (Table S1). There was unambiguous electron density for ligand binding site residues, the bound glutamate molecule and three trapped water molecules in both chains; there was no electron density for residues 416–425, 442–445, and 797–802, in the N terminus, loop 1, and C terminus, respectively. Analysis of the ligand binding site volume was performed using VOIDOO (11) as described previously (6).

1. Petersen SA, Fetter RD, Noordermeer JN, Goodman CS, DiAntonio A (1997) Genetic analysis of glutamate receptors in *Drosophila* reveals a retrograde signal regulating presynaptic transmitter release. *Neuron* 19(6):1237–1248.
2. Serpe M, O'Connor MB (2006) The metalloprotease tolloid-related and its TGF-beta-like substrate Dawdle regulate *Drosophila* motoneuron axon guidance. *Development* 133(24):4969–4979.
3. Kim YJ, Bao H, Bonanno L, Zhang B, Serpe M (2012) *Drosophila* Neto is essential for clustering glutamate receptors at the neuromuscular junction. *Genes Dev* 26(9): 974–987.
4. Zhang W, et al. (2009) A transmembrane accessory subunit that modulates kainate-type glutamate receptors. *Neuron* 61(3):385–396.

5. Panchenko VA, Glasser CR, Partin KM, Mayer ML (1999) Amino acid substitutions in the pore of rat glutamate receptors at sites influencing block by polyamines. *J Physiol* 520(Pt 2):337–357.
6. Mayer ML (2005) Crystal structures of the GluR5 and GluR6 ligand binding cores: Molecular mechanisms underlying kainate receptor selectivity. *Neuron* 45(4):539–552.
7. Otwinowski Z, Minor W (1997) Processing of X-ray diffraction data collected in oscillation mode. *Methods Enzymol* 276:307–344.
8. McCoy AJ, et al. (2007) Phaser crystallographic software. *J Appl Cryst* 40(Pt 4):658–674.
9. Adams PD, et al. (2010) PHENIX: a comprehensive Python-based system for macromolecular structure solution. *Acta Crystallogr D Biol Crystallogr* 66(Pt 2):213–221.
10. Emsley P, Lohkamp B, Scott WG, Cowtan K (2010) Features and development of Coot. *Acta Crystallogr D Biol Crystallogr* 66(Pt 4):486–501.
11. Kleywegt GJ, Jones TA (1994) Detection, delineation, measurement and display of cavities in macromolecular structures. *Acta Crystallogr D Biol Crystallogr* 50(Pt 2): 178–185.

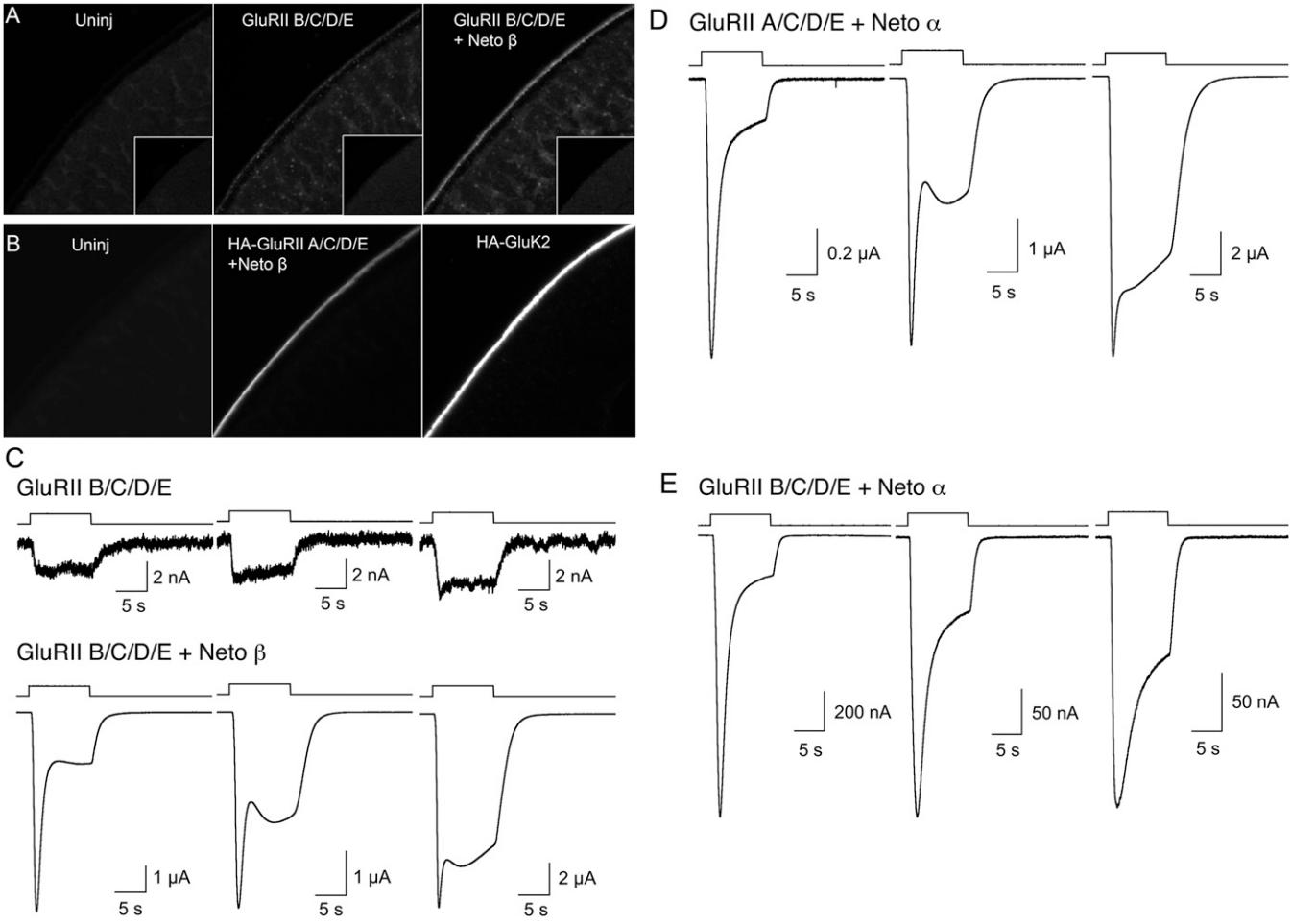

Fig. S1. (*A*) Confocal images of oocytes injected as indicated with cRNA for $RGSH_6$-tagged GluRIIB/C/D/E with or without Neto β, and immunolabeled for anti-$RGSH_6$; the box size for each image is 170 × 170 μm. Surface receptors were detected at the animal but not vegetal pole (*Insets*) and were increased by co-expression of Neto β. (*B*) Confocal images of oocytes injected as indicated with cRNA for HA-tagged GluRIIA/C/D/E plus Neto β or HA-GluK2 and immunolabeled for anti-HA; the box size for each image is 170 × 170 μm. (*C*) Small-amplitude responses to 3 mM glutamate at −60 mV for three representative oocytes injected with cRNA for GluRIIB/C/D/E (*Upper*) and large amplitude responses to 3 mM glutamate at −60 mV (*Lower*) for representative oocytes injected with cRNA for GluRIIB/C/D/E with Neto β, illustrating variability in transient inward current responses. Responses in (*C*) were recorded on the same day from the same batch of oocytes. (*D*) Responses to 3 mM glutamate at −60 mV for three representative oocytes injected with cRNA for GluRIIA/C/D/E and Neto α. (*E*) Responses to 3 mM glutamate at −60 mV for three representative oocytes injected with cRNA for GluRIIB/C/D/E and Neto α. Responses in (*D* and *E*) were recorded on the same day from the same batch of oocytes.

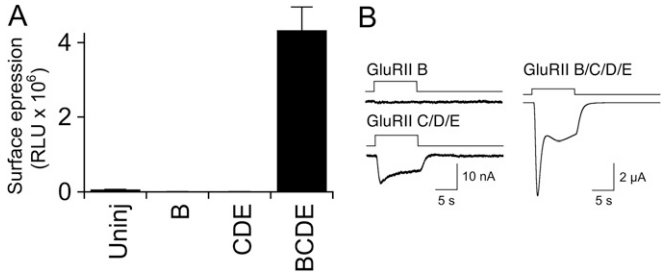

Fig. S2. Subunit dependence of *Drosophila* NMJ glutamate receptor cell surface expression and function. (*A*) Cell surface expression measured by chemiluminescence for different combinations of HA-tagged GluRII subunits; error bars show SEM. (*B*) Responses to 3 mM glutamate at −60 mV for representative oocytes injected with cRNA for GluRIIB, GluRIIC/D/E, and GluRIIB/C/D/E, all recorded on the same day.

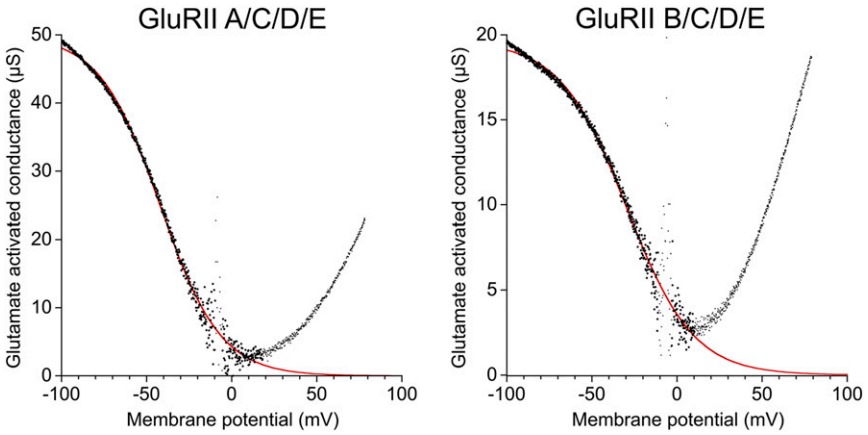

Fig. S3. Typical conductance-voltage plots for GluRIIA/C/D/E and GluRIIB/C/D/E reveal different voltage-dependence for block by cytoplasmic polyamines of GluRIIA- versus GluRIIB-containing receptors; red lines show fits over the range −100 to +20 mV of a Boltzman function of the form

$$G = G_{max}/\left[1 + \exp\left((V_m - V_b)/k_b\right)\right],$$

where G is the conductance at membrane potential V_m; V_b is the potential for half block; and k_b the slope factor. Values for V_b and k_b were −44.8 ± 0.9 mV and 17.6 ± 0.3 ($n = 9$) for GluRIIA/C/D/E and −31.9 ± 1.3 mV and 18.7 ± 0.8 ($n = 10$) for GluRIIB/C/D/E, respectively. The conductance ratio at +80/−80 mV was 44 ± 3% for GluRIIA versus 92 ± 10% for GluRIIB. At the membrane potential for maximum block (V_{min}) the conductance ratio relative to that at −80 mV was 3.3 ± 0.9% for GluRIIA and 9.5 ± 2.9% for GluRIIB, with little difference in the values for V_{min}, 12.4 ± 0.4 mV and 13.7 ± 0.8 mV, respectively.

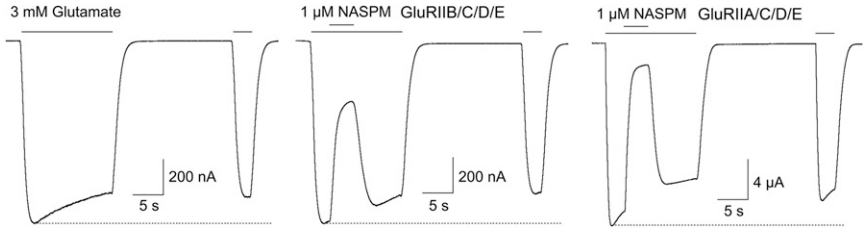

Fig. S4. Correction for rundown for measurement of block by NASPM. (*Left*) Time-dependent rundown for GluRIIB/C/D/E evoked by a 15-s application of 3 mM glutamate, a 20-s pause in control solution, and then a 3-s application of 3 mM glutamate. (*Center*) Recorded from the same oocyte, using the same protocol for application of glutamate, but with a 4-s coapplication of 1 μM NASPM, 3 s after the start of the first application of glutamate. (*Right*) The kinetics of block by 1 μM NASPM for GluRIIA/C/D/E. Measurement of the extent and recovery from block by NASPM was corrected for the rundown measured at the same time points for the control response. The recording for GluRIIB/C/D/E is from the same oocyte illustrating stronger block by 200 nM ATX shown in Fig. 3*G*.

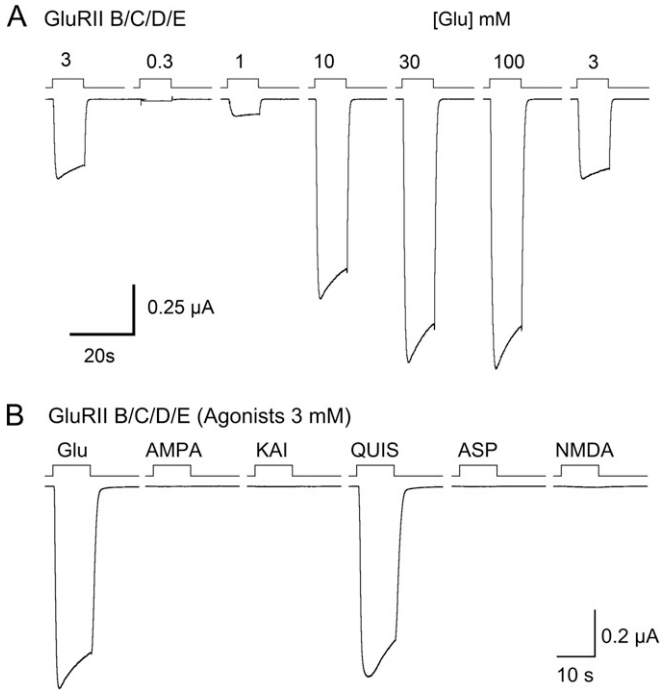

Fig. S5. Agonist sensitivity for GluRIIB responses, (*A*) Typical two-electrode voltage-clamp recordings for GluRIIB/C/D/E showing data for glutamate concentration response analysis. (*B*) GluRIIB/C/D/E responses to six glutamate receptor agonists.

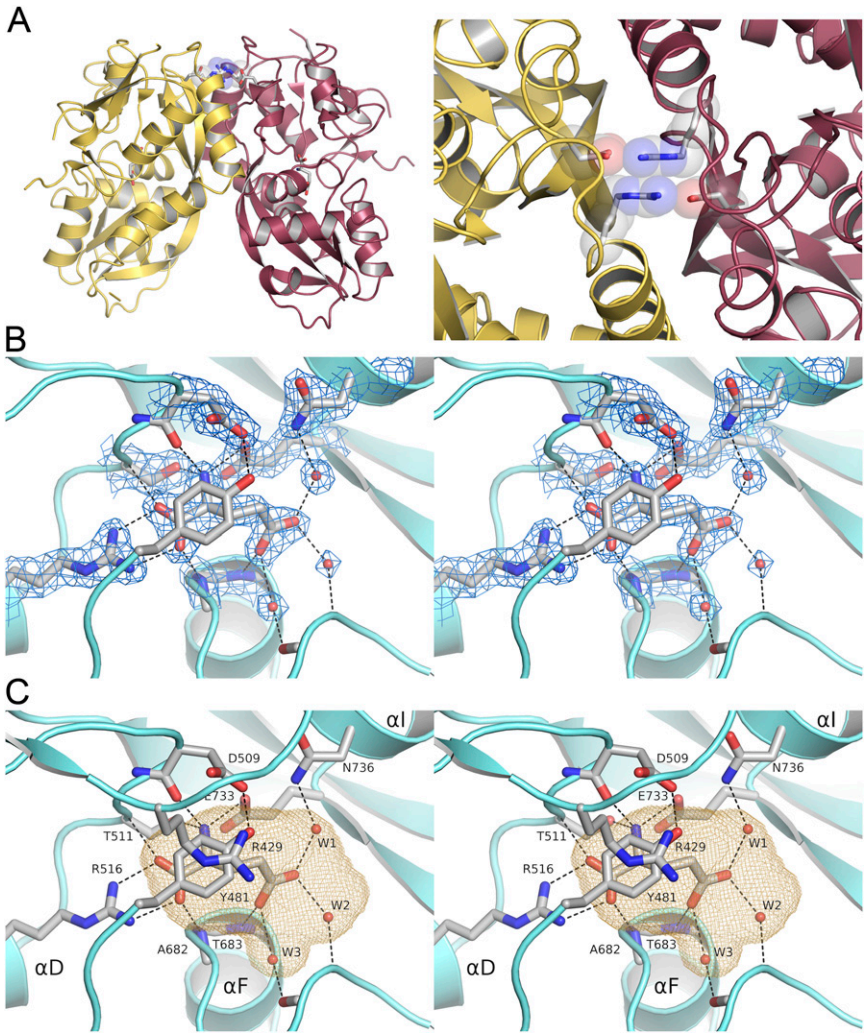

Fig. S6. Crystal structure of the GluRIIB ligand binding domain. (*A*) Side (*Left*) and an expanded top view (*Right*) of the LBD dimer assembly with the two subunits colored gold and magenta, respectively. The side chains for Asp521 and Arg770 are drawn in stick representation, with transparent CPK spheres to highlight an unusual intermolecular stacking of the side-chain guanidinium groups. (*B*) Stereoview of representative electron density for a *2mFo-dFc* map contoured at 2σ showing the glutamate ligand, trapped water molecules and binding-site side chains. (*C*) Stereoview showing capping of the GluRIIB ligand binding site by Arg429, Asp509, and Tyr481, with the cavity containing the ligand and trapped water molecules drawn as an orange mesh.

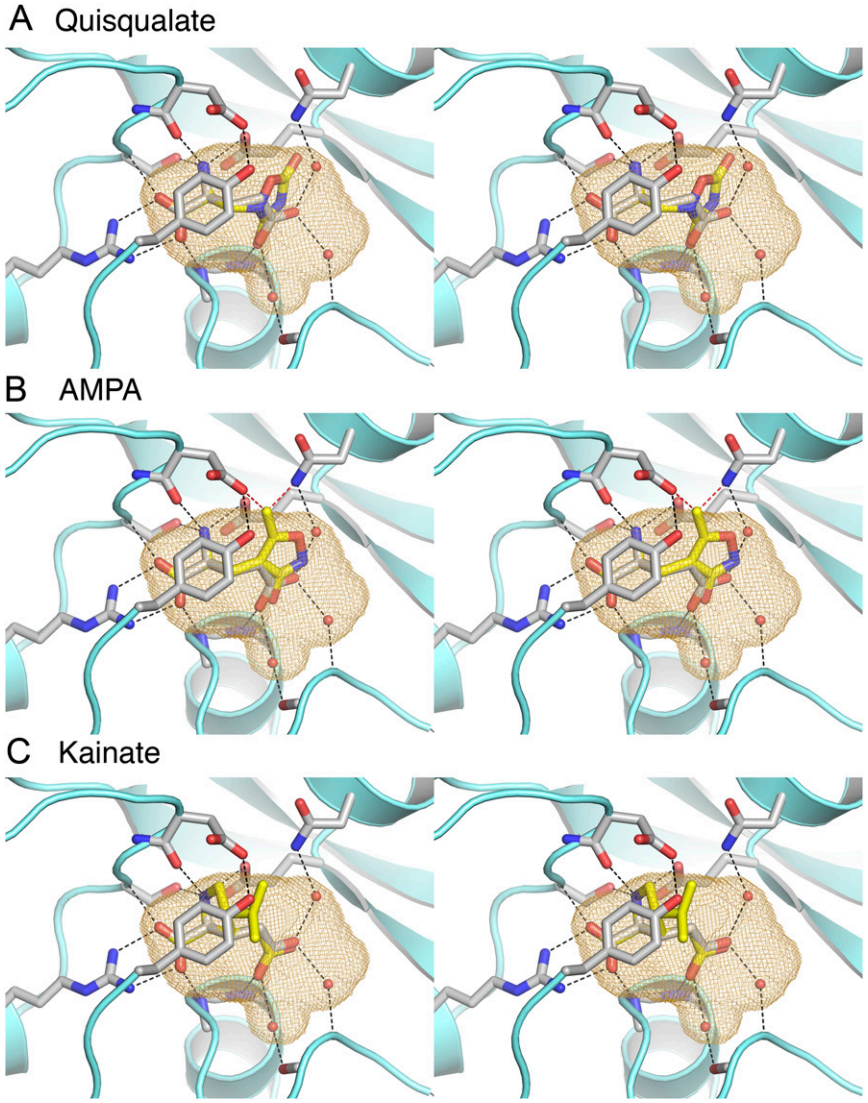

Fig. S7. Stereoviews of the GluRIIB ligand binding domain crystal structure, with structures for (*A*) quisqualate (PDB ID code 1S9T), (*B*) AMPA (PDB ID code 1FTM), and (*C*) kainate (PDB ID code 3C31) superimposed on the bound glutamate ligand by least-squares minimization using ligand N, CA, CB, O, and OXT coordinates. The docked ligands are shown in stick representation using yellow coloring for carbon atoms; the glutamate ligand bound to GluRIIB is shown in stick representation using gray coloring for carbon atoms. Hydrogen bonds with the bound glutamate ligand are shown as black dashed lines; steric clashes are shown as red dashed lines in *B*.

Table S1. Data collection and refinement statistics

Data collection and refinement	Statistics
Data collection	
Space group	$P2_12_12_1$
Unit cell *a, b, c* (Å)	52.3, 94.5, 119.5
$\alpha = \gamma = \beta$	90
Number per AU	2
Wavelength (Å)	1.000
Resolution (Å)*	30.0–2.0 (2.03)
Unique observations	40,664
Mean redundancy†	6.5 (6.3)
Completeness (%)†	99.9 (99.5)
R_{merge}†‡	0.069 (0.84)
R_{pim}†§	0.029 (0.36)
I/σ(I)†	27.6 (2.26)
Refinement	
Resolution (Å)	30.0–2.0 (2.03)
Protein atoms (AC)¶	4,105 (11)
Ligand atoms	20
Water atoms	275
R_{work}/R_{free} (%)‖	20.0/22.9
rms deviations	
Bond lengths (Å)	0.03
Bond angles (°)	0.65
Mean B values *(Å²)*	
Protein overall	33.81
Main chain/side chain	29.6/37.9
Ligand	18.6
Water	34.3
Ramachandran %**	97.8/0.4
PDB ID code	4WXJ

*Values in parenthesis indicate the low resolution limit for the highest-resolution shell of data.

†Values in parenthesis indicate statistics for the highest-resolution shell of data.

‡$R_{merge} = (\Sigma|\ I_i - \langle I_i \rangle|)/\Sigma_i\ |I_i\ |$, where $\langle I_i \rangle$ is the mean I_i over symmetry-equivalent reflections.

§$R_{pim} = (\sqrt{1/(n-1)}\sum_{i=1}^{n}|I_i,I|)/\sum_i I_i$, where $\langle I_i \rangle$ is the mean I_i over symmetry-equivalent reflections.

¶Alternate conformations.

‖$R_{work} = (\Sigma\ ||F_o| - |F_c||)/\Sigma\ |F_o|$, where F_o and F_c denote observed and calculated structure factors, respectively; 5% of the reflections were set aside for the calculation of the R_{free} value.

**Preferred/disallowed conformations.